Application of High-Frequency Ultrasonic Test to the Non-Destructive Inspection of W-Cu Bonded Interface[*]

Noritaka YUSA, Ryouji SUZUKI[1], Takashi FURUKAWA[1],
Masayuki TOKITANI[2] and Suguru MASUZAKI[2]

*Department of Quantum Science and Energy Engineering, Graduate School of Engineering, Tohoku University,
6-6-01-2 Aramaki Aza Aoba, Aoba-ku, Sendai, Miyagi 980-8579, Japan*
[1]*Nondestructive Evaluation Center, Japan Power Engineering and Inspection Corporation,
14-1 Benten-cho, Tsurumi-ku, Yokohama, Kanawaga 230-0044, Japan*
[2]*National Institute for Fusion Science, 322-6 Oroshi, Toki, Gifu 509-5292, Japan*

This study evaluated the applicability of high-frequency ultrasonic tests to the non-destructive inspection of the bonded interface between a cooling pipe and a divertor monoblock. Samples prepared in this study were an ITER-grade tungsten block bonded with a 2.5 mm-thick oxygen-free copper using diffusion bonding. The high-frequency ultrasonic test was performed using an acoustic microscope. A probe, operated in pulse-echo mode, scanned the copper surface of the sample two-dimensionally. Five probes with operating frequencies ranging from 15 to 50 MHz were used. The measured ultrasonic signals were converted into ultrasonic images on the assumption that the samples had a uniform and isotropic speed of sound to evaluate reflections from the interface. Whereas an interface without any artificial flaw partly reflected ultrasonics, setting the decision threshold properly, based on the distribution of the surface echo amplitudes, enabled the smallest flaw to be detected clearly. Ultrasonic signals measured around 30 MHz showed the best signal-to-noise ratio in detecting an artificial flaw introduced at the bonding layer. The results of the ultrasonic tests were consistent with those of subsequent lock-in thermography and destructive test. However the thermography test could not detect small flaws that the high-frequency ultrasonic test confirmed.

1. Introduction

Within a tokamak or a stellarator-type fusion reactor, a divertor plays an important role in exhausting impurity particles and removing the heat load from burning plasma contained in a vessel [1–7]. Because the performance of a divertor is one of the critical issues for ensuring the engineering feasibility and economic efficiency of nuclear fusion reactors to generate electricity, many studies have been conducted to design a divertor. A divertor comprises of a cooling pipe and an armor block that protects the cooling pipe from a huge thermal load. Thus, the pipe and the armor block must be well bonded well so that thermal energies received by the armor block will be effectively transferred to the coolant flowing inside the pipe. Whereas various techniques, including materials for the interlayer, have been proposed for the bonding [8–14], pre-service inspections to confirm the integrity of the bonding are practically indispensable because there is a large number of armor blocks to be bonded with a cooling pipe and the fail-ure of the cooling pipe leads to the coolant leakage into the vacuum vessel.

To detect a flaw hampering heat flux, the thermographic test is the most suitable non-destructive testing method generally, as its signals directly indicate the presence of such a flaw. Several studies have reported the application of the thermographic test to detect a flaw at the bonded interface [15–18]. However, the practical application of the thermographic test to detect a flaw at the interface with a clear thermographic image is challenging because it requires blackening the inner surface of the cooling pipe and inserting an infrared camera into the pipe. Additionally, although a recent study has reported the feasibility of neutron tomography to confirm the minute structure of divertor components three-dimensionally [19], the time necessary for the inspection and activation of the target due to the interaction with neutrons would hamper the application of this technique to inspect all bonded interfaces. Consequently, ultrasonic inspection using a probe inserted into the cooling pipe is regarded as the most promising non-destructive testing method to inspect the bonded interface of a divertor [20–25]. In contrast, however, a few studies

have pointed out that the conventional ultrasonic inspection using a frequency of about 10 MHz would likely be insufficient to evaluate the integrity of the bonding, and another technique with a higher spatial resolution would be necessary [26, 27].

Based on the background above, this study evaluated the applicability of ultrasonic inspection with higher frequencies, specifically those ranging from 15 to 50 MHz. In general, a higher frequency not only leads to a better spatial resolution but also to a larger influence of scattering in ultrasonic tests. Thus, frequencies higher than 15 MHz are seldom used to inspect metallic structural components. However, this also implies that they would be effective for the non-destructive inspection of the bonded interface behind the thin pipe. Samples mimicking the bonding of the coolant pipe were prepared. The results of ultrasonic tests revealed that frequencies around 30 MHz would be suitable for detecting flaws at the interface and have would much better sensitivity against a flaw at the interface than thermographic tests.

2. Sample Preparation

Because various designs have been, and probably will be, proposed for the divertor of a fusion reactor, this study prepared the samples by simplifying one of the fundamental designs of a divertor: tungsten (W) armor bonded with a cooling pipe made of CuCrZr with a 1.5 mm-thick pipe wall, and a 1mm-thick pure copper (Cu) interlayer to mitigate the large thermal expansion coefficient mismatch between the W and CuCrZr.

Figure 1 illustrates a sample prepared in this study. An ITER-grade W block measuring $12.8 \times 26.4 \times 28.4$ mm (W 99.99 wt%) was bonded with an oxygen-free Cu measuring $10 \times 30 \times 30$ mm using a high-temperature vacuum furnace for diffusion bonding (HP-10X10-CC-23, NEMS Co., Ltd., Saitama, Japan). The surfaces to be bonded were polished to a mirror finish using abrasive papers, followed by buff polishing using 3- and 1-micrometer diamond slurries. The temperature, pressure, and time for the bonding are 900 degree Celsius, 10 MPa, and one hour, respectively. The furnace was purged with argon, and the temperature of the furnace was increased from room temperature to the bonding temperature at a speed of 600 degrees Celsius per hour. After a sample was kept at the bonding temperature for one hour, the sample was subjected to furnace cooling. The thickness of the Cu was reduced to 2.5 mm after the bonding to simulate the pipe wall and the interlayer. The roughness of the Cu surfaces, according to JIS B 0601:2011, was approximately $R_a = 3$ μm.

To introduce a flaw at the interface, a flat-bottom drilled hole with a diameter of 1, 3, 5, or 10 mm, and a depth of 0.2 or 0.5 mm was machined at the center of the mirrored surface of the W block. This study used six samples whose specifications are summarized in Table 1.
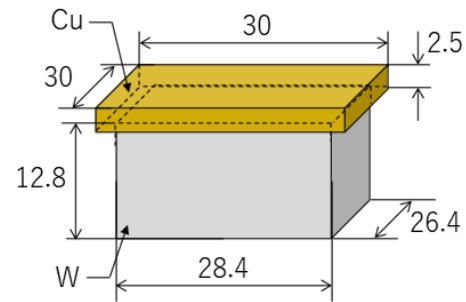
Fig. 1   Profile of the samples (unit: mm).

Table 1   Samples used in this study.

ID	Dimension of a drilled hole at the interface*
TP1	None
TP2	Φ=1 mm, d=0.5 mm
TP3	Φ=3 mm, d=0.2 mm
TP4	Φ=3 mm, d=0.5 mm
TP5	Φ=5 mm, d=0.2 mm
TP6	Φ=10 mm, d=0.5 mm

* Φ and d denote the diameter and the depth, respectively

3. High Frequency Ultrasonic Test
3.1   Experimental setup

The high-frequency ultrasonic test was performed using an acoustic microscope, IS-350 (Insight k.k., Tokyo, Japan). The sample was immersed in water with its Cu surface facing up, and a probe, situated above the sample and operated in pulse-echo mode, scanned the sample two-dimensionally (40 mm $\times 40$ mm) with a pitch of 0.1 mm. To evaluate the effect of frequency, this study used five probes with resonant frequencies of 15, 25, 30, 35, and 50 MHz.

Preferably, the vertical position of a probe should be adjusted so that the W-Cu interface of a sample is focused; however, it is not always easy because the large signal from the surface of the sample sometimes hampers the identification of the signal from the W-Cu interface. Thus, this study adjusted the vertical position of a probe so that the signal from the Cu surface was maximized above the center of the surface and measured each sample twice with different signal amplifications: a small amplification to evaluate the signal from the surface and a large amplification to evaluate that inside the sample. The amplitude of the signal from inside the sample was normalized by the mode of the amplitudes of signals from the surface by postprocessing.

The time-of-flight of the measured ultrasonic signals was converted into the distance from the Cu surface based on their delay from the signal due to the Cu surface. The samples were assumed to have a uniform and isotropic sound speed of 4,660 m/s.

3.2   Results and discussion

Figures 2 and 3 show the C-scan images of signals
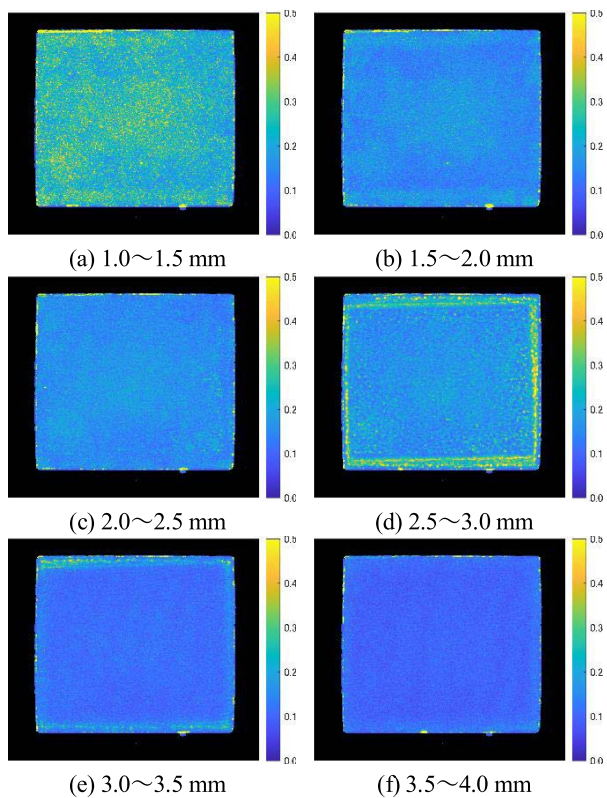
Fig. 2 C-scan images of TP1 measured at 50 MHz. The range in the sub-captions indicates the depth from the copper surface.

Fig. 3 C-scan images of TP4 measured at 50 MHz. The range in the sub-captions indicates the depth from the copper surface.

obtained by measuring TP1 and TP4 with the 50 MHz probe. The amplitudes of the signals in the figures are presented in percentage. Signals under the bonding layer are much weaker than those at and above the layer, which indicates that the W block under the Cu did not cause signals. The relatively larger signals near the edges of the sample, shown in Figs. (d), are caused because the size of the Cu is larger than the W block as illustrated in Fig. 1. Whereas the hole can be confirmed clearly in Figs. 3 (c) and (d), Fig. 2 (d) reveals that non-uniform signals whose amplitudes are almost comparable with those due to the hole are caused at the interface.

To compare the distributions of signals from the bonding interfaces of the samples, Fig. 4 presents histograms of the amplitudes of signals measured at 50 MHz. The histograms are based on signals from a layer whose depth from the Cu surface ranges from 2.0 to 3.0 mm, while signals from near the edges of the Cu are excluded, because they are not from the bonding interface but are caused at the interface between the Cu and water, as mentioned above. Figure 4 (a) shows that the distribution of the signals due to the bonded interface is almost symmetric. In contrast, the distributions shown in Figs. 4 (b) - (f) have longer right tails, while their modes do not differ from the mode presented in Fig. 4 (a). Signals obtained using other frequencies showed the same characteristics. Thus, it would be reasonable to assume that a signal whose am-

plitude significantly differs from the mode of the amplitude of signals obtained from TP1 is caused by the hole at the bonding interface. Therefore, this study regards the mode plus/minus quadruple of the standard deviation of the amplitude of signals from TP1 as thresholds to distinguish signals due to a flaw from noise.

Figures 5 - 11 indicate the locations where the signal amplitudes exceeded the threshold within the scanning area (40 mm × 40 mm). The Cu of TP5 was slightly tilted from the W block due to misalignment in the bonding, which can be confirmed from the image shown in Fig. 9. Figures 5 - 11 reveal that at 15 MHz, the signals from the hole are not always clear because their amplitudes are almost comparable with those from the interface. In contrast, at 50 MHz, although signals due to the holes are clear, there are many indications from the interface. The most plausible reason is that the ultrasonic at 50 MHz is too sensitive and is affected by minute structures. This indicates that using too high a frequency would lead to a larger probability of a false alarm. The results shown in the figures indicate that frequencies around 30 MHz would provide the best signal-to-noise ratio to detect flaws at the bonding interface.

Subsequent image analyses were performed to estimate the size of the holes based on the binary images shown in Figs. 6 - 11. The analyses evaluated the diameters of circles encircling the indications at the center of

(a) TP1   (b) TP2   (c) TP3

(d) TP4   (e) TP5   (f) TP6
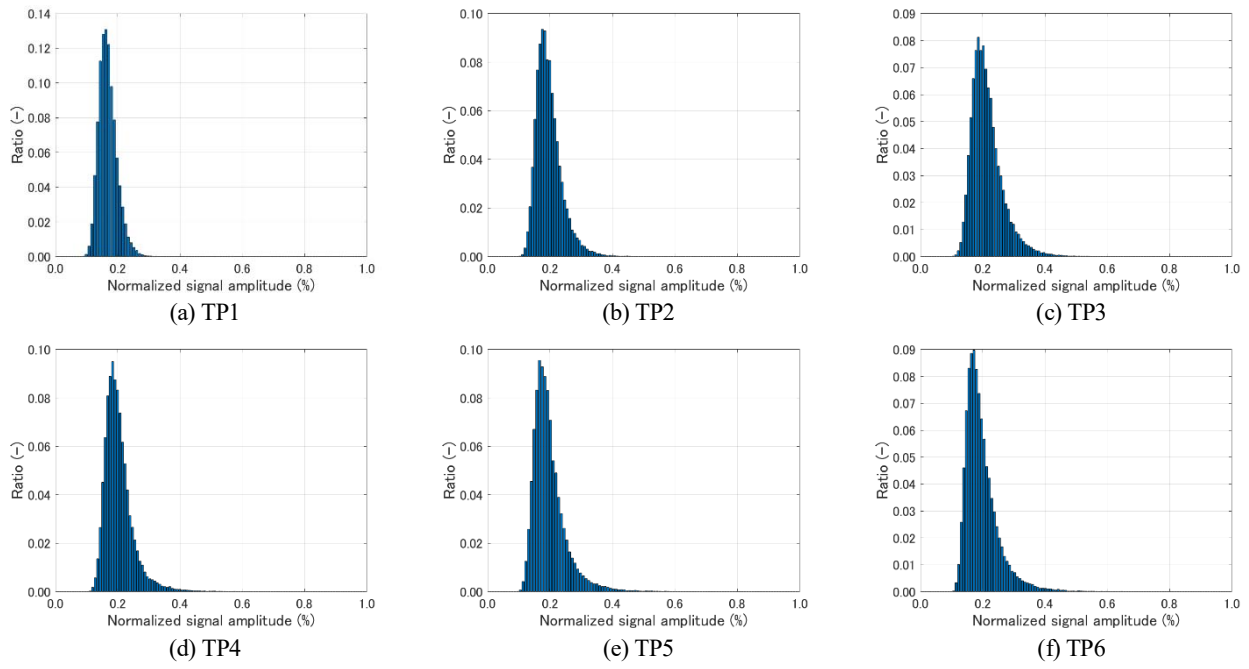
Fig. 4   Histogram of the signal amplitude from $2.0 \sim 3.0$ mm deep, measured at 50 MHz.

(a) 50 MHz   (b) 35 MHz   (c) 30 MHz   (d) 25 MHz   (e) 15 MHz
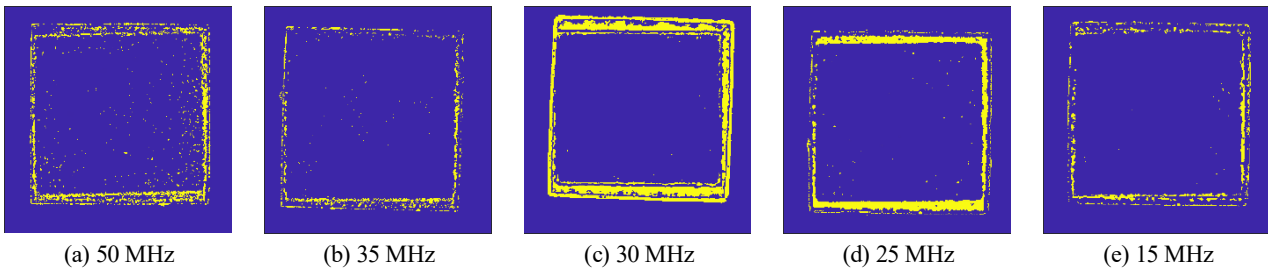
Fig. 5   Locations where signals due to TP1 exceeded the thresholds.

(a) 50 MHz   (b) 35 MHz   (c) 30 MHz   (d) 25 MHz   (e) 15 MHz
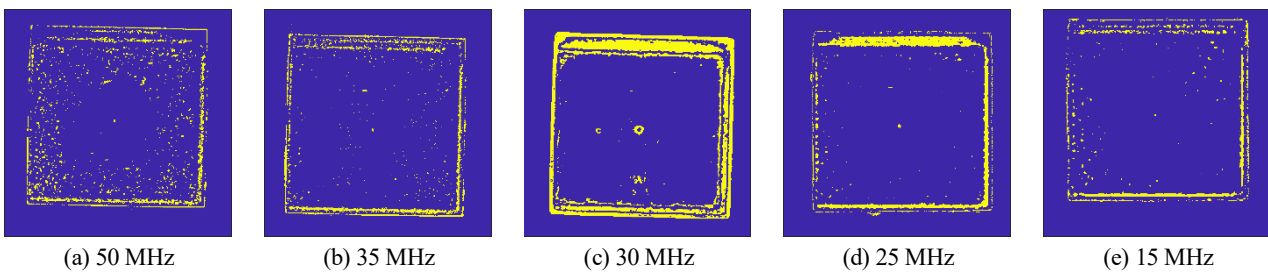
Fig. 6   Locations where signals due to TP2 exceeded the thresholds.

(a) 50 MHz   (b) 35 MHz   (c) 30 MHz   (d) 25 MHz   (e) 15 MHz
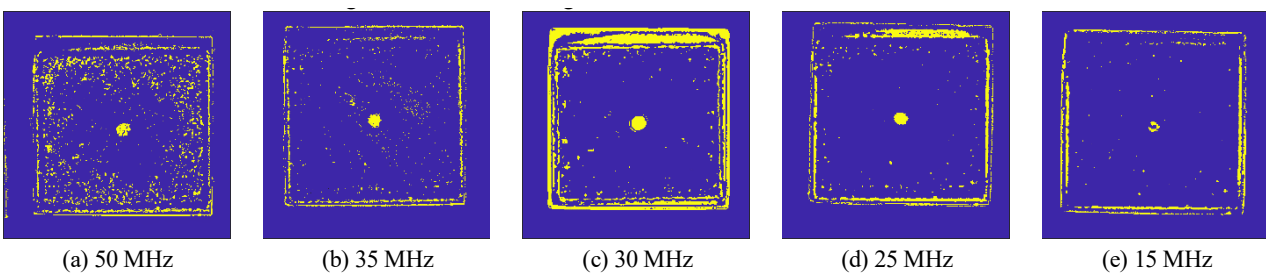
Fig. 7   Locations where signals due to TP3 exceeded the thresholds.

(a) 50 MHz (b) 35 MHz (c) 30 MHz (d) 25 MHz (e) 15 MHz
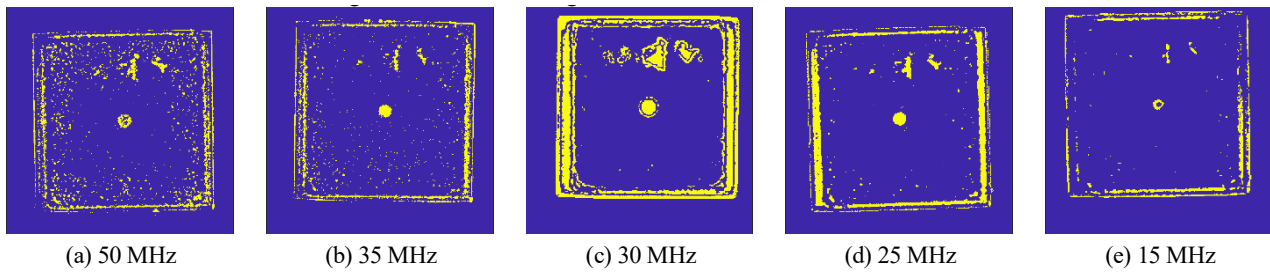
Fig. 8   Locations where signals due to TP4 exceeded the thresholds.

(a) 50 MHz (b) 35 MHz (c) 30 MHz (d) 25 MHz (e) 15 MHz
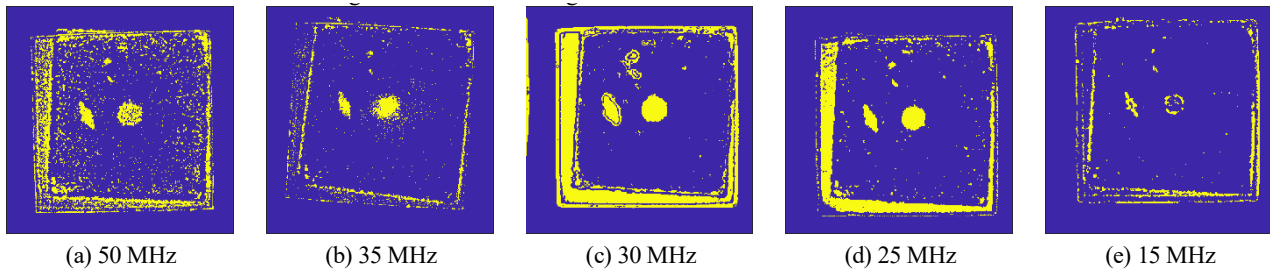
Fig. 9   Locations where signals due to TP5 exceeded the thresholds.

(a) 50 MHz (b) 35 MHz (c) 30 MHz (d) 25 MHz (e) 15 MHz
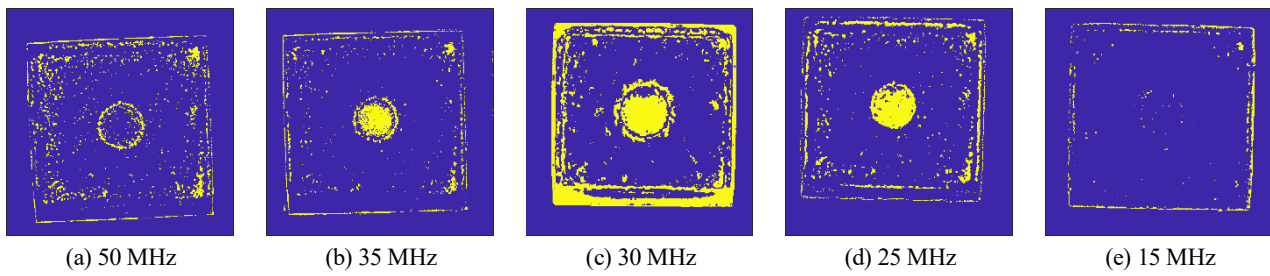
Fig. 10 Locations where signals due to TP6 exceeded the thresholds.

(a) TP1 (b) TP2 (c) TP3

(d) TP4 (e) TP5 (f) TP6
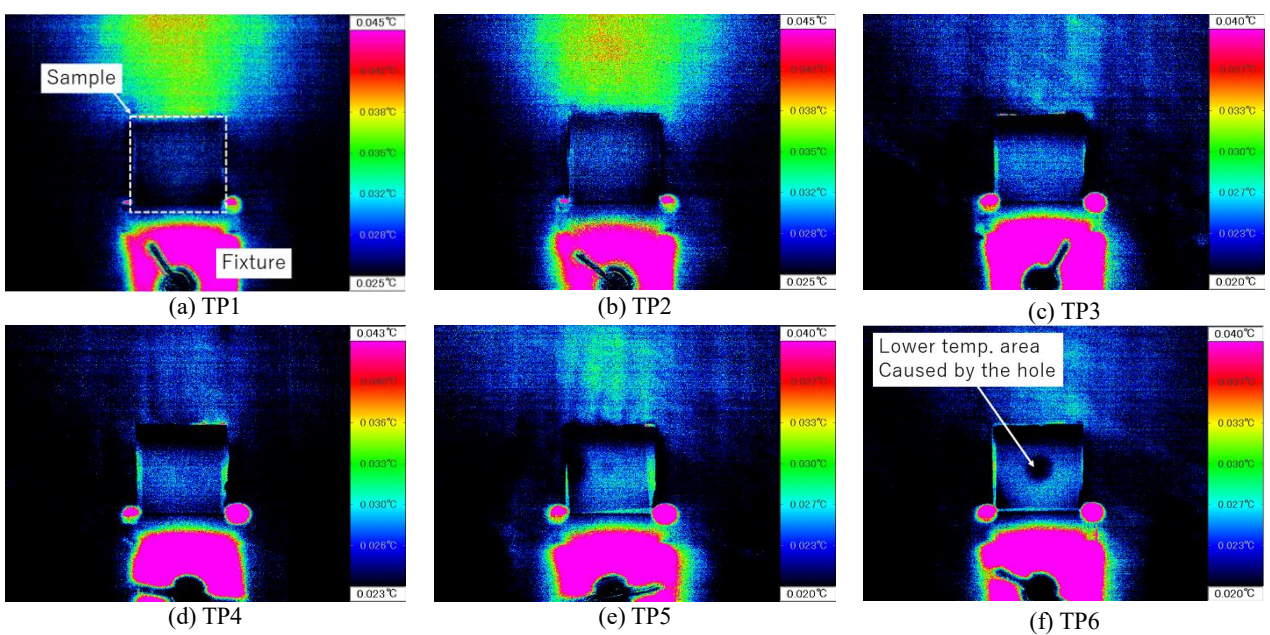
Fig. 11 Results of the thermographic tests.

the images obtained at 30 MHz, whose results evaluated the diameters of the holes in TP2, 3, 4, 5, and 6 were 1.8, 3.2, 3.7, 4.7, and 10.9 mm, respectively. Although the method applied is simple, the error of the evaluation is less than 1 mm. This indicates the possibility of the quantitative evaluation of flaws at the bonded interface using high-frequency ultrasonic tests.

4. Thermographic Test

After the high-frequency ultrasonic test, the samples were machined using electro-discharge machining so that the thicknesses of the Cu and W became 1 mm to make thermographic images from the interface clearer. Subsequently, the surfaces of the samples were blackened to enhance thermal emissivity. The Cu surface of the sample was heated periodically using a halogen lamp, and the temperature distribution of the W surface was measured using an infrared camera (X6580sc, FLIR Systems, USA). Next, the W surface was cooled using a fan, and the camera was synchronized with the heat source to perform lock-in thermography. The resolution, exposure time, and frame rate used to obtain the images were 640×512, 100 μs, and 100 fps, respectively. Based on several preliminary tests, the first 50 frames in each period were used to obtain the thermographic images [28].

Figure 11 presents the thermographic images obtained by the thermographic tests. Samples are situated at the center of the images and the area with a higher temperature at the bottom of each image corresponds to a fixture used to fix the samples, as indicated in Fig. 11 (a). Figure 11 (f) clearly shows the circular area with a relatively low temperature at the center of TP6, which was caused by the hole with a diameter of 10 mm hampering the heat flux; the presence of the hole with a diameter of 5 mm can be confirmed in Fig. 11 (e) whereas it is rather unclear. In contrast, it is difficult to confirm the presence of the flaw in Figs. 11 (b) - (d) as they do not present circular region with a lower temperature clearly unlike Fig. 11 (f), which indicates that the holes with a diameter of 1 and 3 mm were undetectable. Because the thermographic tests were performed after the samples were thinned to 2 mm, the results of the thermographic test support the superiority of the high-frequency ultrasonic tests in detecting a local flaw at the bonded interface.

5. Destructive Test

After the samples were measured using the ultrasonic and thermographic tests, they were subjected to a destructive test to confirm the presence of the holes. The samples were cut at the center using electro-discharge machining, and their cross-sections were polished using abrasive papers, followed by 9-, 3-, and 1-micrometer diamond slurries. Metallographic etching was performed using a mixture of ethanol, hydrochloric acid, and iron (III) chloride.

Figure 12 shows the cross-sectional images of the samples, obtained using a digital microscope (MS-300, Asahikougaku, Tokyo, Japan). The cutting surfaces are parallel to the vertical directions of the images shown in Figs. 5 - 10. The figures confirm that the holes were not deformed significantly, which supports the hypothesis that the indications at the center of the images in Figs. 6 - 10 were caused by the holes, as originally expected. No obvious flaws at the interface can be confirmed, implying that the localized signals notable at 50 MHz stemmed from something different from a flaw at the interface, such as scattering caused by grown crystal grains. In contrast, this is somewhat inconsistent with the presence of the strong signals measured upper part of Fig. 8 (c). The plausible reasons for this are misalignment of the cutting surface, because the area where signals are measured are larger than that of the source as revealed by the image analyses, and/or the signals were caused by a kissing bond that is difficult to be confirmed by an optical microscope. Further metallographic studies are necessary for the quantitative evaluation of the capability of high-frequency ultrasonic tests

6. Conclusion

This study evaluated the feasibility of using a high-frequency ultrasonic test to inspect the bonded interface between the cooling pipe and the divertor monoblock. Because there would be many possible designs of a divertor, this study prepared samples comprising an ITER-grade W block bonded with a 2.5 mm-thick Cu using a hot-press to mimic one of the most fundamental designs of the divertor. High-frequency ultrasonic tests performed using frequencies ranging from 15 MHz to 50 MHz revealed that using a frequency of around 30 MHz provides a good signal-to-noise ratio to confirm the delamination at the interface from C-scan images. The results of the ultrasonic tests were consistent with those of subsequent thermographic and destructive tests, whereas the detectability of the high-frequency ultrasonic test was considerably superior to that of the thermographic test.

It should be noted, however, that this study evaluated the feasibility using a sample that significantly simplified the target. Whereas the results of this study suggest that high-frequency ultrasonic tests, which use a frequency higher than that of conventional ultrasonic tests, are effective for the non-destructive inspection of the bonded interface between the cooling pipe and a divertor armor, the optimum frequency, as well as probe design and signal/image processing methods, should depend on the design of the divertor.

Acknowledgement

(a) TP1

(b) TP2

(c) TP3

(d) TP4

(e) TP5

(f) TP6
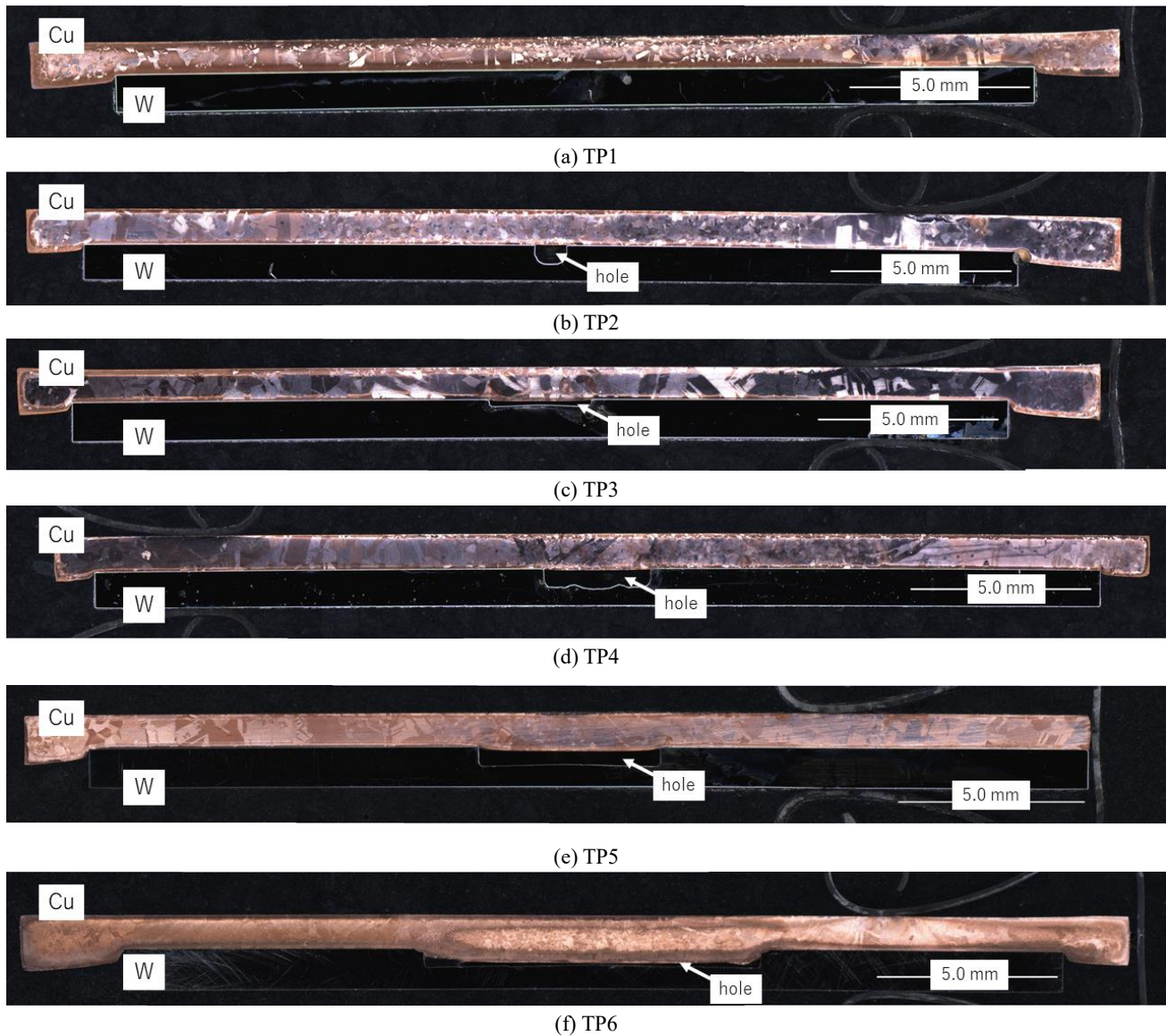
Fig. 12 Cross-sectional images of the samples.

[1] A. Sagara *et al.*, Fusion Eng. Des. **29**, 51 (1995).

[2] A. Loarte, Plasma Phys. Control. Fusion **43**, R183 (2001).

[3] S. Matsuda and K. Tobita, J. Nucl. Sci. Technol. **50**, 321 (2013).

[4] V.P. Budaev, Phys. At. Nucl. **79**, 1137 (2016).

[5] Z. Sun *et al.*, Fusion Eng. Des. **121**, 60 (2017).

[6] J. Linke *et al.*, Matter Radiat. Extremes **4**, 056201 (2019).

[7] R.A. Pitts *et al.*, Nucl. Mater. Energy **20**, 100696 (2019).

[8] V. Barabash *et al.*, J. Nucl. Mater. **283-287**, 1248 (2000).

[9] I.S. Batra *et al.*, Mater. Sci. Eng. **A369**, 119 (2004).

[10] H. Kishimoto *et al.*, Fusion Eng. Des. **136A**, 116 (2018).

[11] W. Liu *et al.*, Fusion Eng. Des. **135A**, 59 (2018).

[12] E. Bang *et al.*, Fusion Eng. Des. **146**, 603 (2019).

[13] D. Mianjun *et al.*, Fusion Eng. Des. **160**, 111813 (2020).

[14] M. Tokitani *et al.*, Nucl. Fusion **61**, 046016 (2021).

[15] N. Vignal *et al.*, Fusion Eng. Des. **88**, 1818 (2013).

[16] X. You *et al.*, J. Fusion Energy **34**, 671 (2015).

[17] Y. Seki *et al.*, Fusion Eng. Des. **85**, 1451 (2010).

[18] Y. Liu *et al.*, IEEE Trans. Plasma Sci. **46**, 1366 (2018).

[19] Ll.M. Evans *et al.*, Fusion Eng. Des. **134**, 97 (2018).

[20] C. Pei *et al.*, Theor. Appl. Mech. Lett. **9**, 180 (2019).

[21] P. Qi *et al.*, Fusion Sci. Technol. **61**, 314 (2012).

[22] G. Dose *et al.*, Fusion Eng. Des. **146**, 870 (2019).

[23] S. Roccela *et al.*, Fusion Eng. Des. **84**, 1639 (2009).

[24] E. Visca *et al.*, Fusion Eng. Des. **136**, 1593 (2018).

[25] M. Fursdon *et al.*, Physica Scripta **T170**, 014042 (2017).

[26] W. Wang *et al.*, Fusion Sci. Technol. **66**, 125 (2014).

[27] N. Mou *et al.*, Fusion Eng. Des. **169**, 112670 (2021).

[28] Japanese Patent No. 6539139.